



HAL
open science

Phase Diagram Structure and Rheology of Boehmite Dispersions: Role of Electrostatic Interactions

Maria Dronova, Eric Lécolier, Loïc Barré, Laurent J. Michot

► **To cite this version:**

Maria Dronova, Eric Lécolier, Loïc Barré, Laurent J. Michot. Phase Diagram Structure and Rheology of Boehmite Dispersions: Role of Electrostatic Interactions. *Colloids and Surfaces A: Physicochemical and Engineering Aspects*, 2021, 631, pp.127564. 10.1016/j.colsurfa.2021.127564 . hal-03544192

HAL Id: hal-03544192

<https://ifp.hal.science/hal-03544192>

Submitted on 26 Jan 2022

HAL is a multi-disciplinary open access archive for the deposit and dissemination of scientific research documents, whether they are published or not. The documents may come from teaching and research institutions in France or abroad, or from public or private research centers.

L'archive ouverte pluridisciplinaire **HAL**, est destinée au dépôt et à la diffusion de documents scientifiques de niveau recherche, publiés ou non, émanant des établissements d'enseignement et de recherche français ou étrangers, des laboratoires publics ou privés.

Phase diagram, structure and rheology of boehmite dispersions: role of electrostatic interactions

Maria Dronova^{a, b}, Eric Lécolier^{a, *}, Loïc Barré^a, Laurent J. Michot^b

^a IFP Energies nouvelles, 1 & 4, Avenue de Bois-Préau, 92852 Rueil-Malmaison, France

^b Laboratoire PHENIX, CNRS-Sorbonne Université UMR8234, 4, place Jussieu, 75005 Paris, France

Keywords:

Boehmite colloids

Sol-gel

Ionic strength, Osmotic pressure

Phase diagram

Small-angle X-ray scattering

Anisotropy

Rheology

ABSTRACT

Improving industrial processes such as filtration of colloidal suspensions requires an in depth understanding of colloidal stability that is linked to interparticle interactions. One way of investigating such phenomena is to determine colloidal phase diagrams and to characterize structure and rheology in various regions of the phase diagrams. Such a strategy was applied in the present paper to the case of boehmite dispersions. The phase diagram of this material, obtained from osmotic stress experiments shows a non trivial behavior, as the sol/gel transition line of boehmite displays a positive slope at low ionic strength and a negative one at higher ionic strength. Combining structural (SAXS) and rheological measurements, it appears that such a behavior can be linked to the ratio between particle anisotropy and Debye length. Such an interpretation is confirmed by modeling the evolution of elastic moduli in various regions of the phase diagram. The model developed takes into account the anisometric nature of particles and provides reasonably accurate predictions of the electrostatic interaction potential in the system.

1. Introduction

Boehmite has been studied for decades owing to its essential industrial importance. In particular, boehmite being a precursor of γ -alumina is widely found in alumina related industries: catalyst carriers, ceramics, metallurgy, treatment of Al-rich radioactive waste. Most boehmite properties are related to its particular structure. Its building structural unit is composed of octahedral double sheets of edge-shared $\text{AlO}_4(\text{OH})_2$ aluminum oxy-hydroxide chains. Two surface oxygen of these layers are linked via hydrogen bonding, which provides a highly polarized, stable hydroxyl-functional surface [1].

Boehmite particles display a wide range of morphology evolving from elongated fibers towards diamond-shaped platelets. As far as synthetic boehmite is concerned, these various particle shapes can be obtained by varying the pH used during synthesis [2,3]. In contrast to clay minerals, boehmite does not present any atomic substitutions yielding structural charge [4] and, consequently the interlayer region between two sheets is free of charge balancing counterions and layer cohesion does not involve electrostatic forces. Despite these structural differences, the rheological properties (shear-thinning, thixotropy,...) of aqueous boehmite dispersions and its phase behavior are somewhat similar to those of clay minerals.

Concerning the phase behavior of boehmite, an isotropic-nematic (I-N) phase transition was observed by Buining and Lekkerkerker, (1993) in the case of highly anisotropic charged boehmite rods [5], whereas gelation with shear induced birefringence was found instead in plate-like boehmite [6]. Apart from the study of Fukasawa and Tsujii [6], the phase behavior of boehmite platelets has scarcely been studied, which appears rather surprising considering the wide use of suspensions of this material in various industrial applications.

In contrast, rheological studies on boehmite dispersions have received more attention [7–13]. One of the earliest attempt to interpret the exceptional stability and elasticity of boehmite dispersions on the basis of the interaction forces between platelets dates back to the 70's and was carried out by Ramsay et al. [9]. Stable boehmite dispersions were found highly elastic and thixotropic, which was assigned to short-range interparticle repulsions. This was indeed evidenced in the work of Karaman et al., (1997) [14] who studied the interactions between alumina coated silica spheres and flat alumina substrates using atomic force microscopy (AFM). In this latter work, the observed repulsion was assigned to natural hydration forces combined with the observation of a gel layer at the alumina surface. Interestingly, the formation of such hydrated gel layer was earlier mentioned by Beattie et al., (1996) [10] who linked it to the presence of mono- or polymeric ionic species that

* Corresponding author.

E-mail address: eric.lecolier@ifpen.fr (E. Lécolier).

condense at the surface and provide repulsion at small interparticle separation distances (< 5 nm).

On the basis of rheometric measurement carried out at different pH and ionic strengths, Evanko et al., (1997) [7] also analyzed the effect of enhanced electrostatic repulsion on the viscosity of concentrated boehmite dispersions. It then appears that particle-particle interactions and bulk rheological behavior are intimately linked and that studying them in parallel could provide viable insight into structure-property relationships.

The present work focuses on platelet-shaped boehmite dispersions and investigates the effect of electrostatic interactions on the phase behavior, structural and rheological properties of these aqueous suspensions. In a first step, boehmite dispersions were equilibrated at fixed ionic strength by osmotic stress experiments to yield the equation of state (osmotic pressure curves vs. solid volume fraction) and phase behavior as a function of both solid volume fraction and ionic strength. The rheological features of the suspensions (in particular yielding and elasticity) were then measured in various areas of the previously determined phase diagrams. In parallel the structure of the suspensions was investigated by small angle X-Ray scattering (SAXS). Based on such information, we attempted to rationalize high frequency elastic moduli on the basis of electrostatic effects in the systems and took into account the anisotropic nature of boehmite particles by using effective volume fractions. In a last step, electrostatic interaction potentials between boehmite particles have been derived.

2. Materials and methods

The present study focuses on an industrial boehmite powder, Pural SB provided by Sasol group (Germany). This is a high purity microcrystalline powder (45 ppm of Fe, 450 ppm of Ti, < 40 ppm of S, < 50 ppm of Cl, < 20 ppm of Na and 0.2 wt% of C) obtained via hydrolysis of aluminum alcoholate in water. Previous X-ray diffraction and small angle X-ray studies [15] revealed the presence of platelet-shaped particles with average length and thickness of 10 nm and 3 nm, respectively. A representative TEM micrograph of the studied boehmite particles is displayed in SP.1 of [supplementary information](#) (see Appendix A) revealing aggregates of slightly anisometric platelets.

Boehmite sols were obtained by peptizing the powder in an aqueous solution containing $0.186 \text{ mol}\cdot\text{L}^{-1}$ of nitric acid at a total solid concentration of $143 \text{ g}\cdot\text{L}^{-1}$. A mixing step using a high-speed disperser (Ultra-Turrax™) was carried out to ensure mechanical breakage of large aggregates into smaller units. Peptization mechanisms of boehmite in the presence of inorganic acids have been largely studied by several research groups [16–18] revealing a complex interaction chemistry at the boehmite – acid interface that results in the formation of colloidal sol. Detailed information about peptization can be found elsewhere [16–18].

The translucent sols thus obtained were then centrifuged at 4 000 g during 4 h in order to eliminate remaining large agglomerates. The resulting supernatant (pH 1.3) was then placed in a porous cellulose membrane with a cut off of 6–8 kDa for dialysis in order to remove ionic species. A buffer reservoir was renewed 1–2 times per week to accelerate the process. The pH of the reservoir was fixed at 5.0–5.2 by adding a few droplets of nitric acid (6.8 wt% HNO_3). The conductivity of the added solution is around 2–3 $\mu\text{S}/\text{cm}$ and the conductivity in the reservoir was then monitored. Renewal by fresh reservoir solution is stopped once the conductivity of the reservoir displays an equilibrium value of 5 $\mu\text{S}/\text{cm}$. Typical total time for such a procedure was around 1–2 months. The volume fraction of the resulting boehmite dispersions after dialysis is $\phi = 0.4 \text{ vol}\%$ ($= 12.7 \text{ g}\cdot\text{L}^{-1}$), and the pH is equal to 6.2.

In order to vary the ionic strength of the suspensions, various amounts of KNO_3 were added into the buffer reservoir at concentrations of $0.0809 \text{ g}\cdot\text{L}^{-1}$ and $1.110 \text{ g}\cdot\text{L}^{-1}$ that corresponds to calculated values of ionic strength $8\cdot 10^{-4} \text{ M}$ and $1\cdot 10^{-2} \text{ M}$, respectively according to

$$I = \frac{1}{2} \sum_{i=1}^n c_i \cdot z_i^2, \quad (1)$$

where c_i is the molar concentration of ions and z_i the number of charges on the ion. The composition of the aqueous phase was analyzed in the following way. Assuming equilibrium inside the dialysis bag and in the buffer reservoir, the latter was used for the analysis of nitrate, potassium and aluminum ions. Measurements were performed by inductively coupled plasma emission spectrometry (ICP-AES) to trace potassium and aluminum and by ion chromatography for nitrate determination.

Suspensions at various ionic strengths were then subjected to osmotic stress experiments. In these tests, cellulose dialysis tubes with a molecular weight cut off of 6–8 kDa were filled with 50 mL of boehmite dispersions and placed in 500 mL tubes containing PEG (MW = 20, 000) solutions at a fixed ionic strength. In such conditions, the relationship between PEG concentration, ϕ_{PEG} , and osmotic pressure, Π , is given by [19].

$$\log_{10} (\Pi_{\text{dyn}\cdot\text{cm}^{-2}}) = 1.57 + 2.57 \cdot (\phi_{\text{PEG}})^{0.21} \quad (2)$$

The duration of the experiment was fixed at 1–2 weeks for boehmite systems, as such duration likely allows reaching osmotic equilibrium. The solid content of the osmotically stressed concentrated dispersions was evaluated by mass balance after drying at 140°C during 24 h.

Optical transparency of diluted boehmite sols after dialysis ($\phi = 0.4 \text{ vol}\%$) enables performing size distribution tests via Dynamic Light Scattering (DLS). These measurements have been carried out on a DLS setup of Cordouan Technologies. The incident beam of a He-Ne laser ($\lambda = 658 \text{ nm}$) passes through the sample in a 10 mm Hellma quartz cuvette. The backscattered light is recorded at 90° by an Avalanche PhotoDiode (APD) detector and used after to build an intensity autocorrelation function $G_2(Q,t)$ (with wave vector Q and time t) to describe fluctuations in scattered light. $G_2(Q,t)$ is related to the modulus of the normalized field autocorrelation function $g_1(Q,t)$ by the Siegert equation

$$G_2(Q,t) = \alpha + \beta g_1^2(Q,t), \quad (3)$$

where α is a baseline and β is the coherence factor.

The time dependence of $g_1(Q,t)$ is essentially linked to the dynamical properties of the given dispersion. In the case of Brownian monodisperse systems, it is described by a single exponential decay, where Γ is the decay rate

$$g_1(Q,t) = \exp(-\Gamma t). \quad (4)$$

For a polydisperse system $g_1(Q,t)$ is written as a sum of exponential decaying functions as

$$g_1(Q,t) = \sum_i A_i \exp(-\Gamma_i t). \quad (5)$$

From the sum of exponential decaying functions, a standard Levenberg-Marquardt is used to adjust the weight of each exponential decaying function. If the studied dispersion is composed by Brownian particles, the diffusion coefficient can be further defined via $\Gamma_i = D_i Q^2$, which enables determining the hydrodynamic radius R_h of the hard sphere-equivalent using Stokes-Einstein equation

$$D_i = \frac{k_B T}{6\pi\eta R_h}, \quad (6)$$

where k_B is the Boltzmann constant and η is the dynamic viscosity of the continuous phase.

The evolution with pH of the zeta potential ζ of suspensions for ionic strengths of $8\cdot 10^{-5} \text{ M}$, $8\cdot 10^{-4} \text{ M}$ and $1\cdot 93\cdot 10^{-3} \text{ M}$ was measured on a

Malvern Nano-ZS zetasizer at ambient temperature. Measurements were carried out without any sample dilution (boehmite concentration of $12.7 \text{ g}\cdot\text{L}^{-1}$). The dispersions were equilibrated for 1 min prior to each measurement. Analysis was repeated 3 times, each measurement cycle was based on over 50–100 runs and averaged.

In the present work, rheological measurements were performed using a Modular Compact rheometer, MCR 302 from Anton Paar instruments equipped with parallel plates geometry. Two plates with a cross-hatched surface were used to avoid wall slip during measurements. The gap between plates was adjusted by controlling the normal force between 2 and 10 N depending on the volume fraction of the samples. Prior to the measurements, the rest interval at the start of the test was set to enable sample relaxation from accumulated internal stresses after setting the gap. Measurements were performed at fixed temperature (20°C). The elastic G' and viscous G'' moduli were measured again in an oscillatory frequency sweep in the range 0.01 – $100 \text{ rad}\cdot\text{s}^{-1}$. A strain of $\gamma = 0.01\%$ was chosen that corresponds to the linear viscoelastic range (LVE), where the storage moduli display constant plateau values. Steady-state viscosity curves were also recorded under controlled shear rate from $1\cdot 10^{-5}$ to 0.1 s^{-1} with a measuring point duration of 5 min.

Small angle X-ray scattering (SAXS) measurements were carried out on boehmite dispersions at room temperature (at 20°C) and without vacuum insulation on beamline SWING at synchrotron SOLEIL. Samples were conditioned between two $50 \mu\text{m}$ Kapton foils. The beam energy was fixed at 12 keV ($\lambda \approx 0.1 \text{ nm}$) and two sample to detector distances (6.2 m and 0.50 m) were used yielding a Q range between $1\cdot 10^{-2}$ and 10 nm^{-1} . The beam size on the sample was approximately $400 \mu\text{m}$ wide and $100 \mu\text{m}$ high. Two-dimensional scattering patterns (typical acquisition times around 1 s) were recorded on an Eiger detector. The curves of scattering intensity versus scattering vector Q , were deduced from azimuthal angular integration of the SAXS patterns. Curves are provided in arbitrary intensity as the thickness of the various samples was not controlled precisely.

3. Results and discussion

3.1. Ionic composition of aqueous phase

The interactions between particles are highly affected by the ionic environment that directly influences the magnitude of electrostatic repulsion. Thus, ionic composition of dialyzed boehmite sols was examined to obtain an accurate determination of ionic strength. The composition of this aqueous phase is defined by (i) dissociation of added salts and (ii) dissolution reactions of alumina species (arising from peptization procedure), whose amount by the end of dialysis becomes negligible. Accordingly, ionic strength can be determined by the concentration of nitrate $[\text{NO}_3^-]$ or potassium $[\text{K}^+]$ ions and the pH given in the exponent, which determines its (ionic strength) order of magnitude (in M)

$$I = \frac{1}{2} ([\text{NO}_3^-] + z_{Al} [\text{Al}] + 10^{-\text{pH}}). \quad (7)$$

The concentration of H^+ ions determined by pH 5.0–5.1 in the buffer dialysis reservoir is $10^{-5} \text{ mol}\cdot\text{L}^{-1}$. The concentration of Al ions is found to be $7\cdot 10^{-5} \text{ mol}\cdot\text{L}^{-1}$, which results in the lowest ionic strength considered in the present study $I_1 = 4\cdot 10^{-5} \text{ mol}\cdot\text{L}^{-1}$. Increase of ionic strength in this “mother” solution was therefore achieved by adding KNO_3 into the buffer reservoir at a given pH. The expression for ionic strength can be rewritten as

$$I = \frac{1}{2} ([\text{NO}_3^-] + [\text{K}^+] + z_{Al} [\text{Al}] + 10^{-\text{pH}}). \quad (8)$$

The detected concentration of ions for intermediate ionic strength is found to be $7\cdot 10^{-4} \text{ mol}\cdot\text{L}^{-1}$ for K^+ ions and $7.5\cdot 10^{-4} \text{ mol}\cdot\text{L}^{-1}$ of NO_3^- ions, resulting in an experimental value of $8\cdot 10^{-4} \text{ mol}\cdot\text{L}^{-1}$ (ionic strength I_2 hereinafter). For the highest ionic strength considered in this

study the measured concentration of ions is $1\cdot 10^{-2} \text{ mol}\cdot\text{L}^{-1}$ for K^+ and NO_3^- ions, leading to a value of $1\cdot 10^{-2} \text{ mol}\cdot\text{L}^{-1}$ (ionic strength I_3 hereinafter).

3.2. Osmotic pressure curves and phase diagram

The osmotic pressure curves and phase diagrams both provide valuable information about the role of interparticle interactions on the resulting structure of particles assembly. Fig. 1 shows the results obtained by osmotic equilibration of dilute boehmite dispersions against PEG solutions of fixed ionic strength at $\text{pH} = 5.0$ – 5.2 . Upon salt addition, the induced electrostatic screening results in a lower osmotic pressure, which is consistent with predictions from DLVO theory. Such an effect is observed for colloidal dispersions whatever the particle shape. In contrast, the presence of a plateau for medium volume fractions and osmotic pressure that is observed in the present case appears to be typical of some plate-like particles. Indeed, it was observed for Na-Wyoming montmorillonite [20] and laponite [21], whereas no plateau was reported in the case of nontronite [22] and beidellite [23] (at least for ionic strengths lower than 10^{-3} M).

The presence of such a plateau might indicate the coexistence of two phases. Indeed, if a phase transition occurs, the osmotic pressure is expected to be equal in both phases which would lead to the appearance of a plateau at the volume fractions separating both phases. This was for instance evidenced in the study of Pages et al. (2008) [24] who suggested that the plateau observed in osmotic pressure curves for an ionic strength of 10^{-3} M can be assigned to the formation of a gel that is kinetically trapped during osmotic stress compression and equilibration. Such a micro-phase separated state was also experimentally evidenced on laponite dispersions using ultra-small angle X-ray scattering experiments (USAXS), displaying a Q^{-3} dependence at low angles [25]. The formation of this latter phase was assigned to the onset of an isotropic/nematic phase transition (Onsager transition), in agreement with numerical predictions for the phase diagram of charged disk-like colloids [26].

To further investigate the system, it is relevant to plot a phase diagram obtained on the basis of rheological measurements that will be detailed later in this paper. Basically at this point, the aim is to distinguish between a free-flowing sol phase and an arrested solid-like phase (which can be named gel as well). A solid-like state refers to a soft solid exhibiting a typical dominance of the storage modulus G' over the loss modulus G'' over the tested frequencies (0.01 – $100 \text{ rad}\cdot\text{s}^{-1}$) and in the linear viscoelastic (LVE) range (see Supplementary Materials SP.2). By applying an increasing mechanical stress, the soft solid starts to flow. On this basis, the resulting phase diagram is plotted in Fig. 2. The dot-

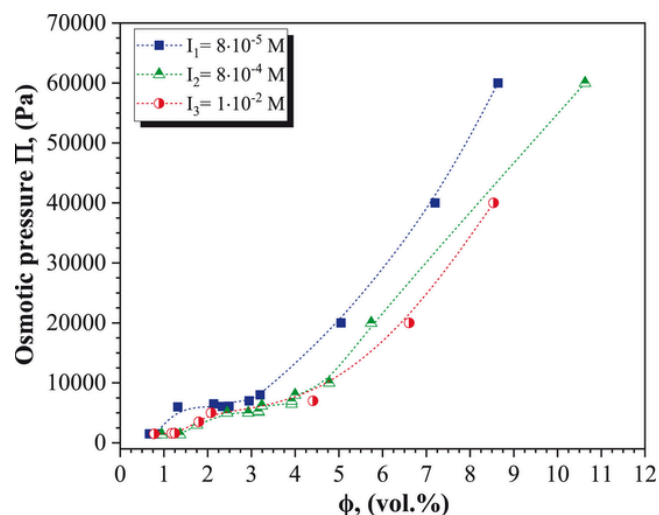


Fig. 1. Equation of state for boehmite dispersions at various ionic strengths.

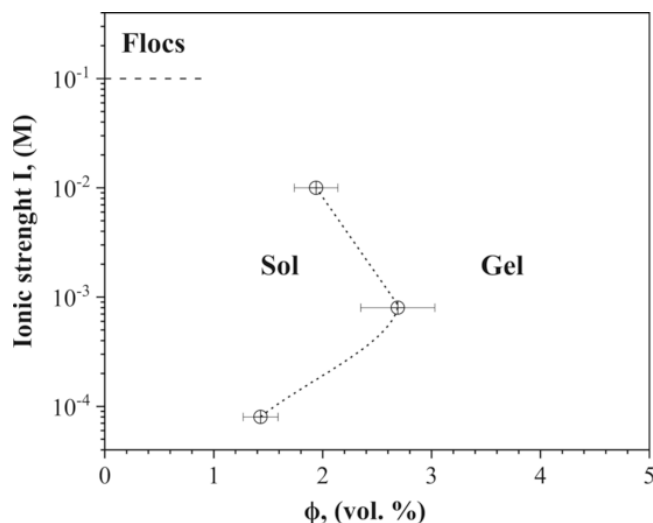


Fig. 2. Rheological phase diagram for boehmite dispersions showing the “>” shape of the sol-gel transition. Boundaries between the sol and gel phases were determined using dynamic oscillation shearing in LVE range.

ted line in this diagram corresponds to the sol-gel transition defined as an average between two distinct points separating the two states. Osmotic pressure with a step of 10 Pa was imposed to ensure the accuracy window accounting for the error of 11–12%. One may notice that the evolution of the sol-gel transition with ionic strength is far from being trivial. Indeed, the sol-gel transition line first exhibits a positive slope up to $8 \cdot 10^{-4}$ M, indicating a system dominated by electrostatic repulsion whereas in the high ionic strength region, i.e. from $8 \cdot 10^{-4}$ M to $1 \cdot 10^{-2}$ M, the slope is reversed. By interpolation, it can be foreseen that this line will join the flocculation line located at high ionic strength (between 0.1 M and 0.15 M, according to [27]). Similar features with a “nose” in the phase diagram have already been observed in other charged anisotropic systems, e.g. synthetic compound laponite [28] or natural clays such as nontronite [29] or beidellite [23].

It must be pointed out that the sol/gel transition in Fig. 2 might coincide with the onset of the plateau in the osmotic pressure curves up to $I_2 = 8 \cdot 10^{-4}$ M, as already observed for laponite [30]. In contrast, such correlation significantly diverges for an ionic strength of $I_3 = 1 \cdot 10^{-2}$ M. It is tempting to attribute this discrepancy to aggregation processes that become apparent at such salinity as will be discussed in more details further in the text.

As already mentioned, the shape of the phase diagram displayed in Fig. 2 is close to the one observed for laponite. In this latter case, the evolution of the gelation mechanism with ionic strength has been highly debated and remains somehow controversial. At very low ionic strength (in the range of the phase diagram with a positive slope) Levitz et al. [31] have shown that the sol-gel transition could be interpreted as a repulsive glass transition (Wigner glass transition) of spherical like objects. According to Wigner predictions, this arises from the long-range Coulombic interactions that block the particles at distances from each other that are much higher than the particle diameter resulting in a solid-like behavior for very small densities as compared to ordinary solids. Along similar lines, based on light scattering tests, Bonn et al. [32] rationalized the dynamics of laponite dispersions at $I \sim 10^{-4}$ M (i.e. just at the “nose” of the transition line) as corresponding to a glassy-like state (which is characterized by no long-range position order and by non-ergodicity), where particles are trapped in cages formed by their neighbors.

For a symmetric monovalent electrolyte, such as KNO_3 , the Debye length κ^{-1} evolves with ionic strength, I , as

$$\kappa^{-1} \text{ (nm)} = \frac{0.304}{\sqrt{I}} \quad (9)$$

In the case of boehmite particles, considering the size of the platelets, i.e. 10 nm, at the lowest ionic strength used in the present work ($8 \cdot 10^{-5}$ M), the corresponding Debye length (≈ 34 nm) is much higher than the average particle size. The particles can then be assimilated to repulsive spheres with a radius of 34 nm forming a gel, once their ionic clouds start interpenetrating each other. Numerical simulations carried out by Jabbari-Farouji et al. [26] suggest that particles immobilized by strong repulsive double-layer interaction (= in the limit of low ionic strengths) can indeed reach a solid-like state with ordered regions. These results are in accordance with data on high-aspect ratio boehmite rods [33] revealing the existence of glassy state that is formed way before the isotropic-nematic (I-N) transition occurs. Moreover, neither the glassy state nor the phase separation was relevant for dispersions containing shorter particles, similarly to our results, suggesting that these processes are presumably driven by excluded volume effects.

In the limit of high ionic strengths, i.e. $I_3 = 1 \cdot 10^{-2}$ M, the Debye length is reduced down to ~ 3 nm in thickness, electrostatic repulsions are strongly screened and Van der Waals forces start playing a major role. Even if the structure of the gel formed in such regions of the phase diagram remains debated, attractive forces likely start playing a role providing an argument in favor of a *percolation* of stacks of platelets [20,34] governed by attraction between edges and faces that results in the so-called “house of cards” configuration. The formation of objects resulting from attraction appears likely in the case of the boehmite suspensions investigated in the present work as (i) suspensions in this region of the phase diagram appear slightly less translucent than those at lower ionic strength, which could well indicate the occurrence of aggregation processes; (ii) these suspensions evolve with time in the long term. Indeed, gel-like behavior appears with time for volume fractions as low as 0.8% but the sample can be reversibly transformed back to sol after gentle shaking. Theoretical works (i.e. [35]) associated with numerical simulations on model clay dispersions suggest various modes of association between platelets when sufficiently high salinity is reached.

In the intermediate region of the phase diagram ($8 \cdot 10^{-4}$ M) the Debye length κ^{-1} is comparable to the length of platelet (~ 10 nm). In this situation, particle anisotropy starts playing a role and long-range interaction with anisotropic short-range excluded interactions both participate in a complex way to the sol-gel transition. Norrish [36] proposed in the 1950’s that gel formation results from the mutual repulsion of particles resulting from interactions between their double layers. Evidence for such processes was provided, for instance, by viscosity tests of Evanko et al. [7] on concentrated alumina dispersions, or by shear stresses and shear moduli measurements on montmorillonite dispersions acquired by Rand et al. [37].

To conclude this section, it appears that a possible interpretation of boehmite phase behavior can be linked to the interplay between particle anisotropy and Debye length resulting in a characteristic sol-gel mechanism given by its delayed appearance at $I_2 = 8 \cdot 10^{-4}$ M as compared to the low and high limits of tested ionic strengths. Therefore, it is tempting to attribute the status of reentrant phase transition at high salt concentration to substantial effect of attraction forces causing clustering effects, as observed by dispersion’s turbidity and time-dependent gelation.

3.3. Structure and particle organization

The structure of dispersions in various zones of the phase diagram was examined by small-angle X-ray scattering in a Q range $1 \cdot 10^{-2}$ and 10 nm^{-1} . The total scattering intensity $I(Q)$ per unit particle volume V is usually expressed as

$$I(Q) = A_e^2 \cdot n_c \cdot V \cdot \Delta\rho^2 \cdot P(Q) \cdot S(Q), \quad (10)$$

where Q is the scattering vector, A_e is the amplitude scattered by one electron, $\Delta\rho^2$ is the electronic density difference between particle and solvent, $P(Q)$ is the form factor and $S(Q)$ the structure factor. In very dilute dispersions, particle interactions are minimized and, in this case, $S(Q)$ is close to unity and the scattering pattern then corresponds to the form factor $P(Q)$. It should be noted, however, that Eq. (10) is valid for identical particles and if particle positions and particle orientations are independent.

Owing to the small anisotropy of boehmite particles, we assume, as first approximation, that the structure factor can be calculated by dividing the scattered intensity by the form factor of the boehmite particle. This calculated structure factor is referred to as an effective structure factor.

A curve corresponding to such a situation ($\phi = 0.2$ vol%) is shown in Fig. 3. At short distances (high Q), the asymptotic decrease in intensity follows a Q^{-4} power law, which is described as the Porod law region dependent on the interfacial area of the solid-liquid interface. At intermediate scattering vector, the intensity decreases as $\approx Q^{-2}$ over a narrow range of Q , suggesting the presence of flat objects characterized by low anisotropy [15]. A similar dependence, but rather more pronounced was constantly reported on several mineral clays, such as lath-shaped nontronite [22] or disk-shaped laponite, which is consistent with scattering expected from the scattering objects displaying bidimensional nature. Interestingly, whatever the ionic strength, at low Q , the intensity keeps on rising, which reveals the presence in the dispersion of a few primary aggregates that dominate the signal at low Q . Note, however, that the curves are not plotted in absolute scale due samples preparation procedure, which prevents a correct fitting of the form factor. Still, previous work on similar particles were plotted in cm^{-1} and were fitted by a form factor corresponding to average particle sizes of $3 \times 32 \times 32$ nm [38]. Comparison between both curves shows that the system studied in the present work is very close to the one already studied.

SAXS patterns were also acquired on boehmite gels concentrated by osmotic stress procedures (also presented in Fig. 3). In such cases, the structure factor $S_{\text{eff}}(Q)$ cannot be neglected and can be experimentally estimated by dividing the intensity obtained for the concentrated dispersion $I(Q)_{\text{conc}}$ by the intensity measured for a dilute non-interacting dispersion $I(Q)_{\text{dil}}$ (volume fraction of 0.2% in the present study), that is to say the single-particle function. The measured intensities were di-

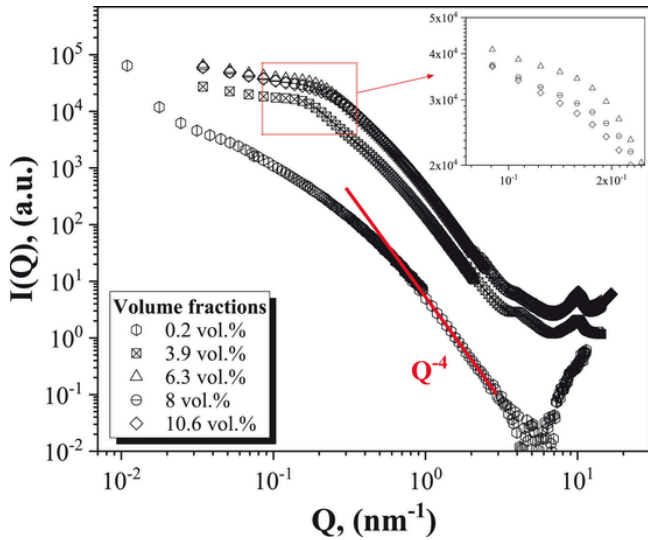


Fig. 3. Example of small-angle X-ray spectra for boehmite dispersions at different volume fractions (ionic strength $I_2 = 8 \cdot 10^{-4}$ M).

vided by the known concentration in both cases in order to exclude the effect of different particle concentrations as

$$S_{\text{eff}}(Q) = \frac{I(Q)_{\text{conc}} \cdot \phi_{\text{dil}}}{I(Q)_{\text{dil}} \cdot \phi_{\text{conc}} \cdot f}. \quad (11)$$

Therefore, Eq. (11) contains an adjustable parameter f to account for the effects linked to the non-constant thickness of the gels analyzed by SAXS.

An example of derived $S(Q)$ in the Q range comprised between 10^{-1} and 1 nm^{-1} is shown in Fig. 4 for boehmite gels prepared at an ionic strength of $8 \cdot 10^{-4}$ M. The positive values of $S_{\text{eff}}(Q)$ regardless of concentration and ionic strength imply a repulsive nature of interparticle interactions in the given boehmite dispersions. Furthermore, the curves display at low Q the presence of a peak, the position of which shifts with volume fraction whereas at high Q , $S(Q)$ approaches unity. The maximum observed is rather broad, which can be linked to the fact that the investigated samples are gels and consequently, rather disordered in terms of particles positions. Still, the position of the maximum of this peak can be used to provide an estimate of the interparticle distance d^* according to

$$d^* = \frac{2\pi}{Q_{\text{max}}}. \quad (12)$$

Fig. 5 displays the evolution with volume fraction of the correlation distances d^* . Various trends can be deduced from this plot. (i) The correlation distances decrease with increasing ionic strength. This is expected and reflects the screening effects of the double layer that results in a shorter distance between particles. Though the data are limited at low volume fractions, it is likely a scaling exponent approaching the value of $-1/3$, which is a typical of an isotropic state. A similar behavior was observed on several clay minerals, such as beidellite and montmorillonite [39], or nontronite [29]. At higher volume fractions, the curves for the $I_1 = 8 \cdot 10^{-5}$ M and $I_2 = 8 \cdot 10^{-4}$ M scale as $\phi^{-0.96}$ and $\phi^{-0.8}$, respectively, suggesting a local lamellar ordering of the platelets. In such a case, the swelling law should be $d^* = t/\phi$, where t is the thickness of individual platelets. Since the thickness of elementary particle is accurately known from earlier studies [15], its integration in the slope fitting in Fig. 5 might suggest the fact of a certain degree of layers exfoliation in the investigated boehmite gels. The transition between both swelling regimes that could indicate the position of a potential isotropic/nematic phase transition is located at volume fractions $\approx 8\%$ and 6% for $I_1 = 8 \cdot 10^{-5}$ M and $I_2 = 8 \cdot 10^{-4}$ M, respectively,

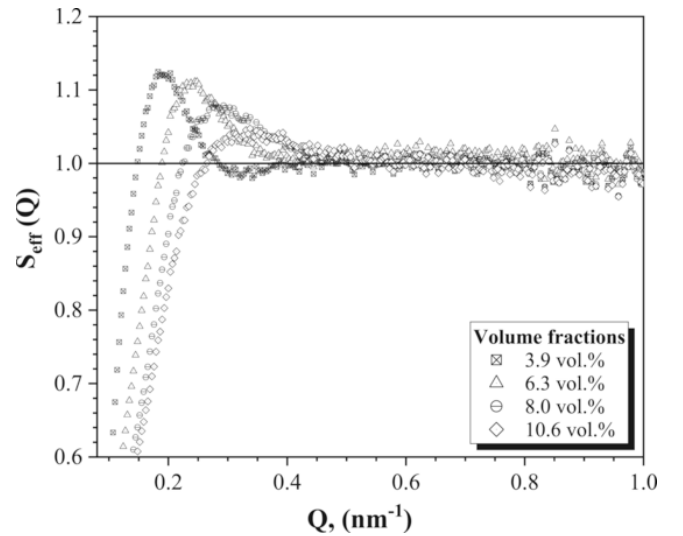


Fig. 4. Structure factor $S_{\text{eff}}(Q)$ for boehmite dispersions at $I_2 = 8 \cdot 10^{-4}$ M and at different volume fractions.

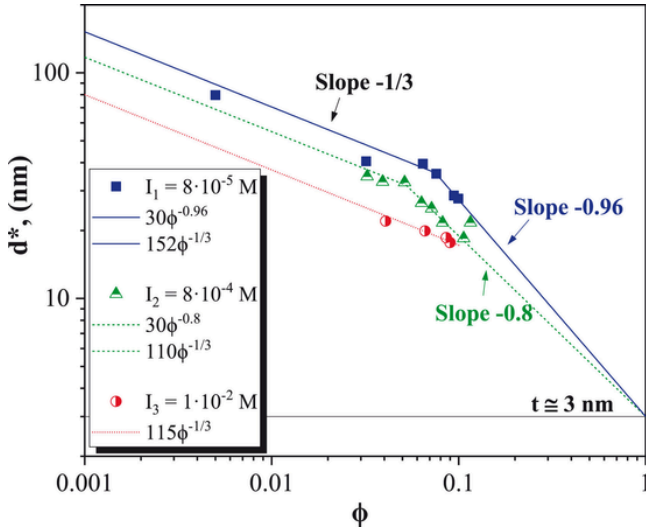


Fig. 5. Evolution of the interparticle distances as a function of volume fraction of boehmite dispersions at various ionic strengths.

i.e. far in the gel region according to the phase diagram of Fig. 2. Consequently, the I/N transition, if present is totally hindered by the sol/gel transition in the boehmite suspensions used in the present study. Notably, several studies on clay mineral have demonstrated that the order-disorder transition does not display a trivial dependence with increasing repulsion. For instance, occurrence in the gel phase of flow-induced birefringence reminiscent of nematic texture has been reported on laponite [30] at lower volume fractions when lowering the ionic strength (in the range of 10^{-2} – 10^{-4} M). Also, aqueous dispersions of gibbsite platelets have revealed that the I-N transition (not hindered by gelation, as in our case) is shifted to higher volume fraction when increasing ionic strength [40]. Another example is the phase diagram of beidellite displaying the similar sol/gel transition line as in our study. However, the narrow regions of a two-phase system and the nematic phase were additionally observed by authors [23] showing dependence on the particle size only, whereas effect of ionic strength was found negligible. Similar trends have been therefore reported on the phase diagram of nontronite [29].

3.4. Elasticity of boehmite gels

The use of oscillatory rheology provides detailed information about the material structure and further illustrates the substantial effect of bulk solution chemistry on interparticles forces. In order to obtain additional information on the suspensions, dynamic moduli were also measured as a function of angular frequency (see [Supplementary Materials SP.3](#)). The evolution of the high frequency elastic modulus G' for different volume fractions and ionic strengths displays a single master curve that follows a power law with a $(\phi - \phi_{\text{sol-gel}})^{1.9}$ dependence (see [Supplementary Materials SP.4](#)). Data points are more scattered at low volume fractions, which is related to the accuracy of the determination of the critical volume fraction corresponding to the sol-gel transition. The data obtained here are similar to those obtained on various clay minerals (laponite [21], nontronite [29], montmorillonite and beidellite [41]) where an exponent of 2.35 was determined.

3.5. Rheological determination of the interaction potential energy

As shown in different publications, the elastic modulus can be used to obtain information about electrostatic interactions in various systems characterized by an elastic response to small deformations, e.g. lattices [42], aqueous clay dispersions [43], sterically stabilized [44] or weakly flocculated systems [45]. Buscall et al. [42] were the first ones

to propose a formula linking the high frequency modulus of a slightly deformed lattice with face-centered cubic symmetry (fcc) and the interaction potential that writes

$$G'_{\infty} = \frac{N\phi_{\text{max}}}{5\pi R} \left[\frac{d^2\psi}{dR^2} \right]. \quad (13)$$

where ψ is the interaction potential, R the center-to-center separation distance between particles, N the coordination number (assuming a f.c.c. packing configuration $N = 12$) and ϕ_{max} the maximal packing ($\phi_{\text{max}} = 0.74$ for f.c.c.).

Eq. (13) therefore illustrates an increasing elastic response originating from enhanced electrostatic interactions (via deformation of the charged ionic clouds surrounding particles) that are governed by the fluctuations of interparticle separation distances during high frequency oscillatory shearing. Since the electrostatic potential increases steeply with decreasing separation distance, this thereby leads to deepen interaction potentials via increasing second derivative of the potential in the vicinity of its minimum (= at the nearest neighbor in contact).

In the case of a mainly repulsive system, neglecting attractive interactions, and in the limit of weak surface potentials and small $\kappa a < 3$ the repulsive potential $\psi(R)$ can be written as [42]

$$\psi(R) = \frac{4\pi\epsilon_r\epsilon_0 a^2 \psi_0^2}{R} \exp(-\kappa(R - 2a)), \quad (14)$$

where a is the sphere radius, ϵ_r the relative permittivity of the electrolyte solution, ϵ_0 the permittivity in the vacuum and ψ_0 the diffuse layer potential defined from ζ -potential measurements. After its differentiation twice and combining with Eq. (13), one then obtains the resulting expression for elastic moduli

$$G'_{\infty} = 4N\phi_{\text{max}}\epsilon_r\epsilon_0 a^2 \psi_0^2 \left(\frac{\kappa^2 R^2 + 2\kappa R + 2}{5R^4} \right) \exp[-\kappa(R - 2a)]. \quad (15)$$

Increasing concentration results in shorter distances between particles and, for spherical objects, the relation between R , a and ϕ can be written as

$$R = 2a \sqrt[3]{\frac{\phi_{\text{max}}}{\phi}}. \quad (16)$$

Since elasticity is linked to a Brownian contribution that acts between particles like elastic springs to restore the microstructure, it is best investigated when the suspension is probed at high frequencies ω (ω is linked to the inverse characteristic relaxation time τ). Therefore, the G' value that must be considered in the above described analysis is the high frequency limit of G' .

In the case of boehmite suspensions, we applied such a procedure to low and intermediate ionic strengths, as for the highest ionic strength ($I_3 = 1 \cdot 10^{-2}$ M), van der Waals attraction is most likely involved, which impairs the analysis.

Two additional points must be considered. (i) charged colloidal particles cannot be considered as hard spheres due to the presence of double layers and (ii) boehmite particles are not spheres. Indeed, the SAXS analysis presented above clearly shows the existence of anisotropic features for boehmite suspensions. Consequently, some additional calculations must be performed before being able to apply Eq. (15) to boehmite dispersions.

Let us first introduce an effective volume fraction ϕ_{eff} defined as

$$\phi_{\text{eff}} = \phi \left(1 + \frac{\alpha}{\kappa a} \right)^3, \quad (17)$$

that depends on the range of electrostatic repulsion through κa and in which α is a scaling parameter accounting for the overlap of double layers. Whereas κa is known, α must be determined. To do this, we assume a classical dependence of viscosity for concentrated suspensions [46] as

$$\eta_r = \frac{\eta_0}{\eta_f} = \left(1 - \frac{\phi}{\phi^*}\right)^{-2}, \quad (18)$$

where η_r is the relative viscosity of the suspension defined as the ratio of its viscosity to the viscosity of the suspending medium and ϕ^* is the maximum packing fraction determined experimentally from rheological tests. According to this equation, for increasing volume fraction, the viscosity of hard spheres dispersions should follow a power law with an exponent of -2 and finally diverge at maximum packing ϕ^* . Fig. 6 presents the evolution of the viscosity of boehmite suspensions obtained for various volume fractions at low and intermediate ionic strengths. The extrapolation of data at zero relative viscosity provides estimates of ϕ^* of 9.6 vol% and 12.1 vol% for ionic strengths of $8 \cdot 10^{-5}$ M and $8 \cdot 10^{-4}$ M, respectively (as shown in Fig. 7).

Further assuming that for particles such as the boehmite used in our study, the maximum volume fraction can be assimilated to $\phi_{\text{eff}}^* = 1$ [43], it is then easy to determine the parameter α in Eq. (17).

Furthermore, for non-spherical particles, the evolution of the inter-particle distance R as a function of volume fraction cannot be described by Eq. (16) and it was shown recently [47] that the following expression applies well to repulsive anisometric particles

$$\langle R \rangle = \frac{2a}{\left(\frac{\phi_{\text{eff}}}{\phi_{\text{eff}}^*}\right)^{1/3} + \left(\frac{\phi_{\text{eff}}}{\phi_{\text{eff}}^*}\right)^n}. \quad (19)$$

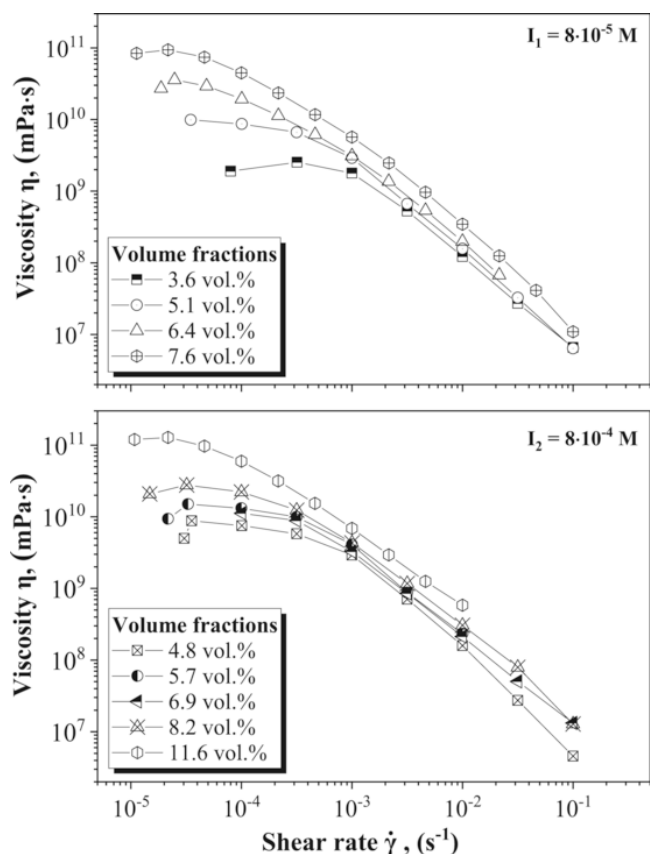


Fig. 6. Zero-shear viscosity curves for colloidal boehmite dispersions at ionic strengths of $8 \cdot 10^{-5}$ M and $8 \cdot 10^{-4}$ M (steady shear flow measurements).

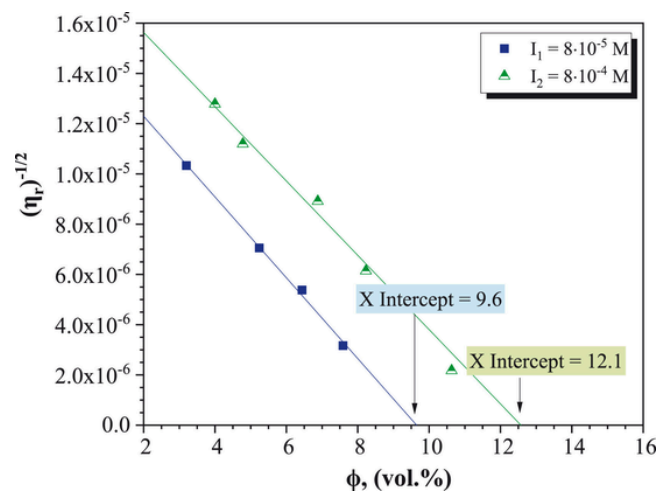


Fig. 7. Determination of experimental maximum packing fraction for colloidal boehmite dispersions at ionic strengths of $8 \cdot 10^{-5}$ M and $8 \cdot 10^{-4}$ M.

The term in the denominator in Eq. (19) provides the harmonic average between the isotropic state at low volume fractions and the organized state in the limit of high concentrations. The parameter n can be directly obtained from SAXS data (fitting slopes from Fig. 5) and in our case, values of 0.96 and 0.8 were taken for ionic strengths of $8 \cdot 10^{-5}$ M and $8 \cdot 10^{-4}$ M, respectively.

Fig. 8 compares the experimental data obtained for G' with the predictions made on the basis of Eq. (13). An increase in ionic strength leads to a decrease of G' , a trend that was already observed for PBMA systems [44] and polystyrene lattices [48]. It is worth noting that for the disordered state, the maximum packing number N is no longer valid. Horn et al. [49] has applied instead the perturbation theory of Bergenholtz et al. [44] by considering a pair distribution function $g(r)$ that reflects the spatial configuration of particles, displaying a pronounced sharp maximum at the nearest neighbor distance. In a similar way, since the plateau moduli were measured for highly concentrated gels, where particles display locally 2D stacking (Fig. 5), in this case, as a

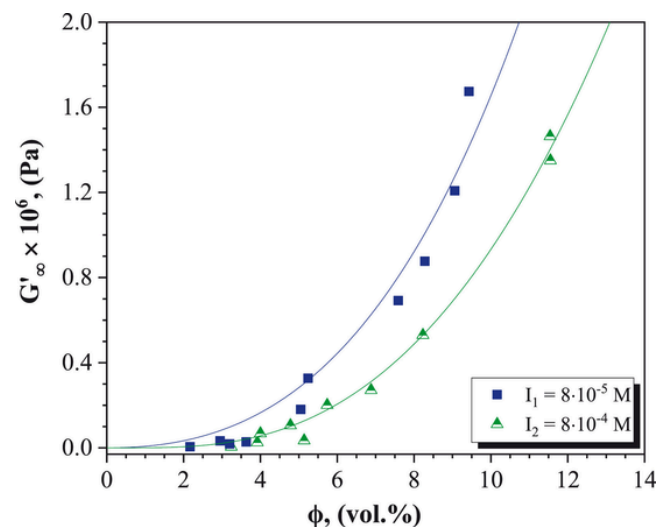


Fig. 8. High frequency elastic modulus as a function of the volume fraction for boehmite gels at different ionic strengths. The solid lines correspond to the fitting as discussed in the text according to Eq. (15) with effective volume fraction ϕ_{eff} given by Eq. (17). The effective maximum packing ϕ_{eff}^* is taken 1. The zeta potentials are $\psi_0 = 187$ mV for $I_1 = 8 \cdot 10^{-5}$ M and $\psi_0 = 56$ mV for $I_2 = 8 \cdot 10^{-4}$ M. The reciprocal Debye length κ^{-1} calculated from Eq. (9) is set 34 nm and 10.75 nm for $I_1 = 8 \cdot 10^{-5}$ M and for $I_2 = 8 \cdot 10^{-4}$ M, respectively. $N = 6$.

first approximation, N can be fixed to 6 by assuming the repulsive contribution of all six face-face platelet configurations.

Using radii of 30 – 20 nm for $I_1 = 8 \cdot 10^{-5}$ M and $I_2 = 8 \cdot 10^{-4}$ M, respectively, a reasonable fit of G' data is obtained (Fig. 8). Therefore, such values of a appear in close accordance with DLS measurements, presented in supplementary information (Appendix E, SP.6). It must be pointed out though that such values are average values whereas the actual particles likely display significant polydispersity.

Remarkably, for the lowest ionic strength it can be seen that the zeta values are over predicted by a factor of 3 in comparison with experimental ζ data acquired for diluted suspensions (see Supplementary Materials in Appendix D, SP.5). This may be well a consequence of the constraints of Eq. (14) for repulsive interaction potential $\psi(R)$, which is applicable only in the limit of weak surface potentials ($\psi_0 < 50$ mV) [42].

Further tests of the values obtained by fitting G' values can be obtained by comparing the evolution with volume fractions of distance $\langle R \rangle$ obtained by SAXS with those derived from applying Eq. (19) as displayed in Fig. 9. The results agree fairly well, values calculated from Eq. (19) being higher than experimental data by a few %. Considering the complexity¹ of the system under investigation, such a result is truly convincing. The systematic slight overestimation of calculated values could be due to an overestimation of the effective volume fraction that could be related to the choice that was made to fix ϕ_{eff}^* at 1.

Considering the satisfactory fit between experimental and calculated values displayed in Fig. 9, Eq. (19) can be used for determining the interaction potential according to Eq. (14). The results of such a calculation are displayed in Fig. 10. For all the regimes investigated in the present study, the electrostatic potential is higher than the energy $k_B T$ of thermal fluctuations by at least a factor of 20. The potential decays rapidly with increasing surface separation and increasing ionic strength decreases the electrostatic, which concurs with the electrical double layer concept. As this model was successfully applied to montmorillonite disk-like particles [43], the results presented in our study strongly suggest that the methodology used here could really be fruitful for analyzing correlations between electrostatic effects and viscoelastic properties in colloidal suspensions of anisometric particles.

4. Conclusion and perspectives

Studying in details the phase diagram, rheology and structure of industrial boehmite suspensions comprised of plate-like particles has provided a consistent picture of the impact of interparticle interactions on gelation mechanisms, viscoelastic properties and structural features. In terms of phase diagram, distinct ranges of interactions modulated by salt addition have been revealed. Indeed, the transition line separating liquid suspensions from gel phases exhibits a change of slope from positive to negative when increasing ionic strength, a behavior similar to that observed for other plate-like charged colloids (i.e. laponite [31] or nontronite [29]). This slope inversion occurs at an ionic strength value ($I = 8 \cdot 10^{-4}$ M), for which the corresponding Debye length becomes comparable with the platelet size. Structural analysis by small angle X-ray scattering has therefore evidenced local nematic ordering far above the sol-gel transition, likewise on different clay minerals [29,39]. Still no isotropic/nematic transition was observed for boehmite, in contrast with what was found for aqueous dispersions of gibbsite [50] or small aspect ratio nontronite [29]. The sol/gel transition appears to hinder the I/N transition, a feature that was also observed on numerous anisotropic systems such as montmorillonite [20] or laponite [21]. The features revealed in the present paper may help in rationalizing these different situations on the basis of particle anisotropy and ionic strength. Lastly, by coupling rheological measurements with structural

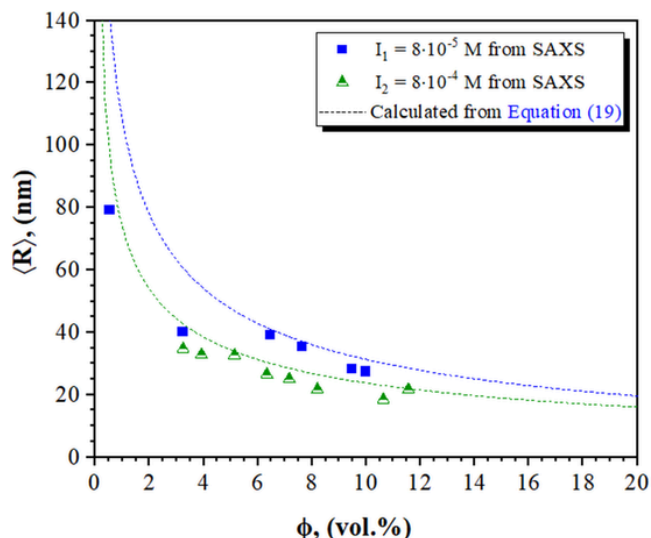


Fig. 9. Evolution of the interparticle distance with volume fraction of boehmite gels.

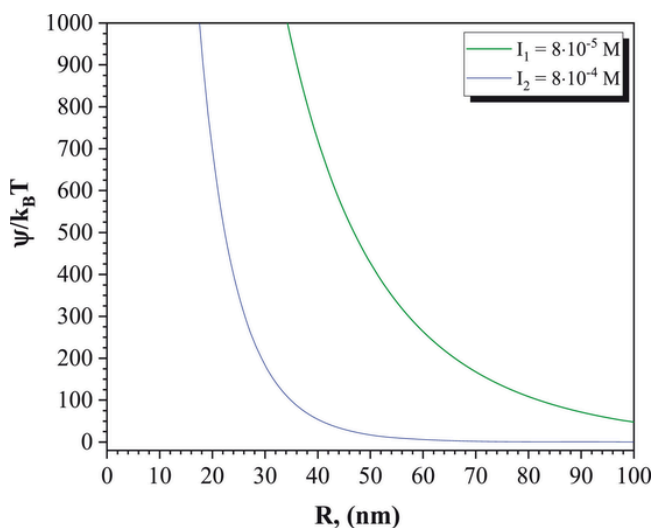


Fig. 10. Estimated electrostatic potential for boehmite dispersions at ionic strengths of $8 \cdot 10^{-5}$ M and $8 \cdot 10^{-4}$ M from Eq. (14), using values of interparticle distance (R) determined from calculations, Eq. (19), experimentally measured zeta potentials ψ_0 and values of a as mentioned in the text.

information obtained by SAXS measurements, we were able to extend the approach initially developed by Buscall et al. [42] to the case of boehmite platelets displaying moderate polydispersity. An effective volume scaling accounting for excluded volume effects due to induced orientational and rotational motion of particles allows capturing interactions over a wide range of particle concentrations and in the limit of moderate ionic strengths before aggregation processes comes into effect. We could thus rationalize rheological data on the basis of the electrostatic interactions in the system, which provides a coherent picture of viscoelastic properties with regard to increasing volume fraction and ionic strength.

The use of such a model should be further examined on experimental data of other anisotropic systems to reinforce its validity. This could also be completed by taking into account electroviscous effects that were neglected in the present approach [51]. Additional static and dynamic birefringence measurements could also provide clearer information about the nematic ordering of platelets and future work could certainly focus on coupling rheological experiments with scattering measurements. This would strengthen the analysis of flow induced orienta-

¹ The complexity of the system stems from the particles polydispersity presented in Appendix A (TEM micrograph) and Appendix E (DLS measurements).

tion which might lead to changes in processing condition upon filtration of such “complex” colloidal suspensions.

CRedit authorship contribution statement

Maria Dronova: Investigation, Formal analysis, Conceptualization, Writing – original draft. **Eric Lécolier:** Conceptualization, Validation, Writing – review & editing, Supervision. **Loïc Barré:** Investigation, Supervision. **Laurent J. Michot:** Conceptualization, Investigation, Writing – review & editing, Supervision.

Declaration of Competing Interest

The authors declare that they have no known competing financial interests or personal relationships that could have appeared to influence the work reported in this paper.

Acknowledgements

We thank Mrs Palazzo (IFPEN) for technical assistance in samples preparation, Dr D. Frot for DLS measurements and Dr V. Rouchon (IFPEN) for TEM observations. We would like to thank synchrotron SOLEIL for beamtime allocation.

Appendix A. Supporting information

Supplementary data associated with this article can be found in the online version at [doi:10.1016/j.colsurfa.2021.127564](https://doi.org/10.1016/j.colsurfa.2021.127564).

References

- J.D. Russell, V.C. Farmer, D.G. Lewis, Lattice vibrations of boehmite (γ -AlOOH): evidence for a C122v rather than a D172h space group, *Spectrochim. Acta Part A* 34 (12) (1978) 1151–1153, [https://doi.org/10.1016/0584-8539\(78\)80073-7](https://doi.org/10.1016/0584-8539(78)80073-7).
- J.-P. Jolivet, S. Cassaignon, C. Chanéac, D. Chiche, E. Tronc, Design of oxide nanoparticles by aqueous chemistry, *J. Sol. -Gel Sci. Technol.* 46 (3) (2008) 299–305, <https://doi.org/10.1007/s10971-007-1645-4>.
- X. Zhang, W. Cui, K.L. Page, C.I. Pearce, M.E. Bowden, T.R. Graham, Z. Shen, P. Li, Z. Wang, S. Kerisit, A.T. N'Diaye, S.B. Clark, K.M. Rosso, Size and morphology controlled synthesis of boehmite nanoplates and crystal growth mechanisms, *Cryst. Growth Des.* 18 (6) (2018) 3596–3606, <https://doi.org/10.1021/acs.cgd.8b00394>.
- M. Conroy, J.A. Soltis, R.S. Wittman, F.N. Smith, S. Chatterjee, X. Zhang, E.S. Ilton, E.C. Buck, Importance of interlayer H bonding structure to the stability of layered minerals, *Sci. Rep.* 7 (1) (2017) 13274, <https://doi.org/10.1038/s41598-017-13452-7>.
- P.A. Buining, H.N.W. Lekkerkerker, Isotropic-nematic phase separation of a dispersion of organophilic boehmite rods, *J. Phys. Chem.* 97 (44) (1993) 11510–11516, <https://doi.org/10.1021/j100146a027>.
- J.-I. Fukasawa, K. Tsujii, Higher-order structure formation of ultrafine boehmite particles in sols, gels, and dried materials, *J. Colloid Interface Sci.* 125 (1) (1988) 155–161, [https://doi.org/10.1016/0021-9797\(88\)90064-1](https://doi.org/10.1016/0021-9797(88)90064-1).
- C.R. Evanko, R.F. Delisio, D.A. Dzombak, J.W. Novak, Influence of aqueous solution chemistry on the surface charge, viscosity and stability of concentrated alumina dispersions in water, *Colloids Surf. A* 125 (2–3) (1997) 95–107, [https://doi.org/10.1016/S0927-7757\(96\)03574-5](https://doi.org/10.1016/S0927-7757(96)03574-5).
- J.S. Weston, J. Chun, G. Schenter, K. Weigandt, M. Zong, X. Zhang, K.M. Rosso, L.M. Anovitz, Connecting particle interactions to agglomerate morphology and rheology of boehmite nanocrystal suspensions, *J. Colloid Interface Sci.* 572 (2020) 328–339, <https://doi.org/10.1016/j.jcis.2020.03.109>.
- J.D.F. Ramsay, S.R. Daish, C.J. Wright, Structure and stability of concentrated boehmite sols, *Faraday Discuss. Chem. Soc.* 65 (1978) 65, <https://doi.org/10.1039/DC9786500065>.
- J.K. Beattie, J.K. Cleaver, T. Waite, Anomalous aggregation behaviour of aluminium oxyhydroxides, *Colloids Surf. A* 111 (1–2) (1996) 131–138, [https://doi.org/10.1016/0927-7757\(95\)03493-5](https://doi.org/10.1016/0927-7757(95)03493-5).
- K. Strengé, U. Bollmann, A rheological investigation of peptized boehmite suspensions, *Colloids Surf.* 57 (1) (1991) 139–148, [https://doi.org/10.1016/0166-6622\(91\)80186-R](https://doi.org/10.1016/0166-6622(91)80186-R).
- C. Cristiani, A. Grossale, P. Forzatti, Study of the physico-chemical characteristics and rheological behaviour of boehmite dispersions for dip-coating applications, *Top. Catal.* 42–43 (1–4) (2007) 455–459, <https://doi.org/10.1007/s11244-007-0224-9>.
- J. Drouin, T. Chopin, P. Nortier, H. van Damme, Rheology and structure of peptized boehmite pastes, *J. Colloid Interface Sci.* 125 (1) (1988) 314–326, [https://doi.org/10.1016/0021-9797\(88\)90080-X](https://doi.org/10.1016/0021-9797(88)90080-X).
- M.E. Karaman, R.M. Pashley, T.D. Waite, S.J. Hatch, H. Bustamante, A comparison of the interaction forces between model alumina surfaces and their colloidal properties, *Colloids Surf. A* 129–130 (1997) 239–255, [https://doi.org/10.1016/S0927-7757\(97\)00040-X](https://doi.org/10.1016/S0927-7757(97)00040-X).
- F. Mange, D. Fauchadour, L. Barré, L. Normand, L. Rouleau, A microstructural investigation of nanostructured boehmite films prepared by the sol-gel route, *Colloids Surf. A* 155 (2–3) (1999) 199–210, [https://doi.org/10.1016/S0927-7757\(98\)00856-5](https://doi.org/10.1016/S0927-7757(98)00856-5).
- C. Cristiani, M. Valentini, M. Merazzi, S. Neglia, P. Forzatti, Effect of ageing time on chemical and rheological evolution in γ -Al₂O₃ slurries for dip-coating, *Catal. Today* 105 (3–4) (2005) 492–498, <https://doi.org/10.1016/j.cattod.2005.06.020>.
- Fauchadour D., Kolenda F., Rouleau L., Barré L., Normand L., Peptization mechanisms of boehmite used as precursors for catalysts, in *Scientific Bases for the Preparation of Heterogeneous Catalysts - Proceedings of the 8th International Symposium, Louvain-la-Neuve, Belgium 9–12, 2002*. Elsevier, 2000, 453–461.
- Y. Zheng, J. Song, X. Xu, M. He, Q. Wang, L. Yan, Peptization mechanism of boehmite and its effect on the preparation of a fluid catalytic cracking catalyst, *Ind. Eng. Chem. Res.* 53 (24) (2014) 10029–10034, <https://doi.org/10.1021/ie501060g>.
- Harries Daniel. (<https://scholars.huji.ac.il/danielharries/book/peg-20k>).
- L.J. Michot, I. Bihannic, K. Porsch, S. Maddi, C. Baravian, J. Mougel, P. Levitz, Phase diagrams of Wyoming Na-montmorillonite clay. Influence of particle anisotropy, *Langmuir* 20 (25) (2004) 10829–10837, <https://doi.org/10.1021/la0489108>.
- A. Mourchid, A. Delville, J. Lambard, E. Lécolier, P. Levitz, Phase diagram of colloidal dispersions of anisotropic charged particles: equilibrium properties, structure, and rheology of laponite suspensions, *Langmuir* 11 (6) (1995) 1942–1950, <https://doi.org/10.1021/la00006a020>.
- L.J. Michot, I. Bihannic, S. Maddi, C. Baravian, P. Levitz, P. Davidson, Sol/gel and isotropic/nematic transitions in aqueous suspensions of natural nontronite clay. Influence of particle anisotropy. 1. Features of the i/n transition, *Langmuir* 24 (7) (2008) 3127–3139, <https://doi.org/10.1021/la703506z>.
- E. Paineau, K. Antonova, C. Baravian, I. Bihannic, P. Davidson, I. Dozov, M. Impérator-Clerc, P. Levitz, A. Madsen, F. Meneau, L.J. Michot, Liquid-crystalline nematic phase in aqueous suspensions of a disk-shaped natural beidellite clay, *J. Phys. Chem. B* 113 (48) (2009) 15858–15869, <https://doi.org/10.1021/jp908326y>.
- M.G. Page, T. Zemb, M. Dubois, H. Cölfen, Osmotic pressure and phase boundary determination of multiphase systems by analytical ultracentrifugation, *Chemphyschem* 9 (6) (2008) 882–890, <https://doi.org/10.1002/cphc.200700668>.
- J.M. Saunders, J.W. Goodwin, R.M. Richardson, B. Vincent, A small-angle X-ray scattering study of the structure of aqueous laponite dispersions, *J. Phys. Chem. B* 103 (43) (1999) 9211–9218, <https://doi.org/10.1021/jp9907185>.
- S. Jabbari-Farouji, J.-J. Weis, P. Davidson, P. Levitz, E. Trizac, On phase behavior and dynamical signatures of charged colloidal platelets, *Sci. Rep.* 3 (2013) 3559, <https://doi.org/10.1038/srep03559>.
- D. Fauchadour, *Etude de la peptisation de la boehmite* (2000).
- C. Martin, F. Pignon, J.-M. Piau, A. Magnin, P. Lindner, B. Cabane, Dissociation of thixotropic clay gels, *Phys. Rev. E Stat. Nonlinear Soft Matter Phys.* 66 (2 Pt 1) (2002) 21401, <https://doi.org/10.1103/PhysRevE.66.021401>.
- L.J. Michot, C. Baravian, I. Bihannic, S. Maddi, C. Moyné, J.F.L. Duval, P. Levitz, P. Davidson, Sol-gel and isotropic/nematic transitions in aqueous suspensions of natural nontronite clay. Influence of particle anisotropy. 2, *Gel Struct. Mech. Prop. Langmuir* 25 (1) (2009) 127–139, <https://doi.org/10.1021/la801894a>.
- A. Mourchid, E. Lécolier, H. van Damme, P. Levitz, On viscoelastic, birefringent, and swelling properties of laponite clay suspensions: revisited phase diagram, *Langmuir* 14 (17) (1998) 4718–4723, <https://doi.org/10.1021/la980117p>.
- P. Levitz, E. Lécolier, A. Mourchid, A. Delville, S. Lyonnard, Liquid-solid transition of Laponite suspensions at very low ionic strength: Long-range electrostatic stabilisation of anisotropic colloids, *EPL (Europhys. Lett.)* 49 (5) (2000) 672–677, <https://doi.org/10.1209/epl/i2000-0203-9>.
- D. Bonn, H. Tanaka, G. Wegdam, H. Kellay, J. Meunier, Aging of a colloidal “Wigner” glass, *EPL (Europhys. Lett.)* 45 (1) (1999) 52–57, <https://doi.org/10.1209/epl/i1999-00130-3>.
- A. Wierenga, A.P. Philipse, H.N.W. Lekkerkerker, D.V. Boger, Aqueous dispersions of colloidal boehmite: structure, dynamics, and yield stress of rod gels, *Langmuir* 14 (1) (1998) 55–65, <https://doi.org/10.1021/la970376z>.
- B. Ruzicka, E. Zaccarelli, A fresh look at the Laponite phase diagram, *Soft Matter* 7 (4) (2011) 1268, <https://doi.org/10.1039/c0sm00590h>.
- M. Delhomme, B. Jönsson, C. Labbez, Monte Carlo simulations of a clay inspired model suspension: the role of rim charge, *Soft Matter* 8 (37) (2012) 9691, <https://doi.org/10.1039/C2SM25731A>.
- K. Norrish, The swelling of montmorillonite, *Discuss. Faraday Soc.* 18 (1954) 120, <https://doi.org/10.1039/DF9541800120>.
- B. Rand, E. Pekenč, J.W. Goodwin, R.W. Smith, Investigation into the existence of edge-face coagulated structures in Na-montmorillonite suspensions, *J. Chem. Soc. Faraday Trans. 1* 76 (0) (1980) 225, <https://doi.org/10.1039/F19807600225>.
- C. Morin, Préparation d’alumine à porosité contrôlée: étude de l’interaction de la boehmite dans des solvants et des propriétés fonctionnelles des matériaux résultants, *Université Pierre et Marie Curie - Paris VI* (2014).
- E. Paineau, I. Bihannic, C. Baravian, A.-M. Philippe, P. Davidson, P. Levitz, S.S. Funari, C. Rochas, L.J. Michot, Aqueous suspensions of natural swelling clay minerals. 1. Structure and electrostatic interactions, *Langmuir* 27 (9) (2011) 5562–5573, <https://doi.org/10.1021/la2001255>.
- D. van der Beek, H.N.W. Lekkerkerker, Nematic ordering vs. gelation in suspensions of charged platelets, *EPL (Europhys. Lett.)* 61 (5) (2003) 702–707, <https://doi.org/10.1209/epl/i2003-00132-1>.
- E. Paineau, L.J. Michot, I. Bihannic, C. Baravian, Aqueous suspensions of natural swelling clay minerals. 2. Rheological characterization, *Langmuir* 27 (12) (2011) 7806–7819, <https://doi.org/10.1021/la2001267>.

- [42] R. Buscail, J.W. Goodwin, M.W. Hawkins, R.H. Ottewill, Viscoelastic properties of concentrated latices. Part 2.—Theoretical analysis, *J. Chem. Soc., Faraday Trans. 1* 78 (10) (1982) 2889, <https://doi.org/10.1039/F19827802889>.
- [43] C. Baravian, D. Vantelon, F. Thomas, Rheological determination of interaction potential energy for aqueous clay suspensions, *Langmuir* 19 (19) (2003) 8109–8114, <https://doi.org/10.1021/la034169c>.
- [44] J. Bergenholtz, N. Willenbacher, N.J. Wagner, B. Morrison, D. van den Ende, J. Mellema, Colloidal charge determination in concentrated liquid dispersions using torsional resonance oscillation, *J. Colloid Interface Sci.* 202 (2) (1998) 430–440, <https://doi.org/10.1006/jcis.1998.5463>.
- [45] J.W. Goodwin, R.W. Hughes, S.J. Partridge, C.F. Zukoski, The elasticity of weakly flocculated suspensions, *J. Chem. Phys.* 85 (1) (1986) 559–566, <https://doi.org/10.1063/1.451580>.
- [46] D. Quemada, Rheology of concentrated disperse systems and minimum energy dissipation principle, *Rheol. Acta* 16 (1977) 82–94.
- [47] C. Baravian, L.J. Michot, E. Paineau, I. Bihannic, P. Davidson, M. Impéror-Clerc, E. Belamie, P. Levitz, An effective geometrical approach to the structure of colloidal suspensions of very anisometric particles, *EPL (Europhys. Lett.)* 90 (3) (2010)
- [48] D. Benzing, W. Russel, The viscoelastic properties of ordered lattices: experiments, *J. Colloid Interface Sci.* 83 (1) (1981) 178–190, [https://doi.org/10.1016/0021-9797\(81\)90022-9](https://doi.org/10.1016/0021-9797(81)90022-9).
- [49] F.M. Horn, W. Richtering, J. Bergenholtz, N. Willenbacher, N.J. Wagner, Hydrodynamic and colloidal interactions in concentrated charge-stabilized polymer dispersions, *J. Colloid Interface Sci.* 225 (1) (2000) 166–178, <https://doi.org/10.1006/jcis.1999.6705>.
- [50] M.C.D. Mourad, D.V. Byelov, A.V. Petukhov, D.A. Mattheijs de Winter, A.J. Verkleij, H.N.W. Lekkerkerker, Sol-gel transitions and liquid crystal phase transitions in concentrated aqueous suspensions of colloidal gibbsite platelets, *J. Phys. Chem. B* 113 (34) (2009) 11604–11613, <https://doi.org/10.1021/jp903783b>.
- [51] D. Quemada, C. Berli, Energy of interaction in colloids and its implications in rheological modeling, *Adv. Colloid Interface Sci.* 98 (1) (2002) 51–85, [https://doi.org/10.1016/S0001-8686\(01\)00093-8](https://doi.org/10.1016/S0001-8686(01)00093-8).